Structure and magnetism of $MnMgB_2O_5$ and $Mn_2B_2O_5$

J. C. Fernandes, F. S. Sarrat, R. B. Guimarães, R. S. Freitas, and M. A. Continentino*
Instituto de Física, Universidade Federal Fluminense, Campus da Praia Vermelha, Niterói, 24210-340 Rio de Janeiro, Brazil

A. C. Doriguetto, Y. P. Mascarenhas, J. Ellena, and E. E. Castellano
Instituto de Física de São Carlos, Universidade de São Paulo, Caixa Postal 369, São Carlos, São Paulo 13560-970, Brazil

J-L. Tholence and J. Dumas
Laboratoire d'Etudes des Propriétés Electroniques des Solides, CNRS, BP 166, 38042 Grenoble Cedex 9, France

L. Ghivelder
Instituto de Física, Universidade Federal do Rio de Janeiro, CP 68528, Rio de Janeiro, 21945-970 Rio de Janeiro, Brazil
(Received 22 October 2002; published 17 March 2003)

We present an investigation of the magnetic properties of the pyroborates $Mn_2B_2O_5$ and $MnMgB_2O_5$ using magnetization and electron-paramagnetic-resonance measurements. The pyroborates have in common with another well studied family of borates, the warwickites, substructures in the form of *ribbons* where the metals are located. The homometallic $Mn_2B_2O_5$ system is shown to be a conventional three-dimensional antiferromagnet with Neel temperature $T_N \approx 24$ K. Its magnetization isotherms present steps indicating spin-flop-like transitions involving distinct pairs of metal sites. The heterometallic compound $MnMgB_2O_5$ shows a susceptibility with a power-law temperature dependence $\chi(T) \propto T^{-\alpha}$, down to $T = 1.8$ K and a magnetization with a power-law field dependence $M(H) \propto H^{(1-\alpha)}$ at low temperatures. This behavior is characteristic of a random singlet phase, in this case, in a system with spin $S = 5/2$. We discuss our magnetic results on the pyroborates in connection with their structure and compare them with those obtained in the warwickites.

DOI: 10.1103/PhysRevB.67.104413 PACS number(s): 75.20.Ck, 61.10.Nz, 75.60.Ej, 76.30.−v

I. INTRODUCTION

This work presents an experimental investigation of the structural and magnetic properties of the *pyroborates* $Mn_2B_2O_5$ and $MnMgB_2O_5$. The pyroborates are compounds with chemical formula $MM'B_2O_5$ where M or M' stands for Mg, Ca, or a divalent $3d$ transition metal. Their crystalline structure is triclinic with space group $P-1$ (number 2).[1] The metals M and M' are found inside oxygen octahedra that shares edges and form substructures like *ribbons*, four rows wide, as shown in Fig. 1. These ribbons are parallel to the crystallographic *a axis* and contain two different sites for the metal ions. The boron ions have trigonal coordination forming borate groups $B_2O_5^{4-}$ as shown in Fig. 2. The five oxygen ions of each borate group belong to three distinct ribbons as indicated in Fig. 1.

Within the framework of the magnetism of the borates, it is interesting to compare the behavior of the pyroborates with that of the *warwickites*, a group of oxy-borates with chemical formula $MM'OBO_3$ that has been intensively studied.[2–5] The crystalline structure of the latter is orthorhombic and also contains four rows wide ribbons with two different crystallographic sites for the metal ions.[4] In the warwickites, however, there are some oxygen sites which are common to two distinct ribbons. In the pyroborates, we remark, the ribbons do not *touch* each other (see Fig. 1). Another difference between both structures is shown by the borate groups: in the warwickites the boron coordination is also trigonal but the borate group composition is BO_3^{3-} with each oxygen on a different ribbon.[4] Among their magnetic properties, the *homometallic* warwickites Mn_2OBO_3 and Fe_2OBO_3 behave as three-dimensional (3D) antiferromagnets which order at 104 K and 155 K, respectively.[5] Besides, both materials present weak ferromagnetism in the ordered state. On the other hand, the *heterometallic* warwickites $MnScOBO_3$ and $MgFeOBO_3$ have magnetic susceptibilities characteristic of low-dimensional disordered magnets, with a power-law behavior with temperature as expected for a

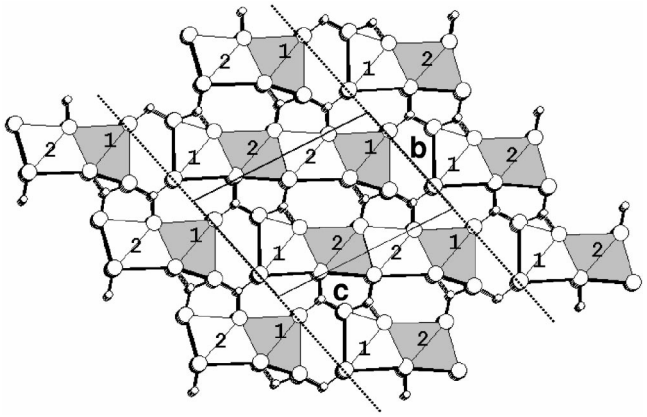

FIG. 1. The structure of the pyroborates projected in the plane bc. We may notice the ribbons, the borate groups, and the sides b and c of the unit cell. The largest circles indicate oxygen ions while the smallest ones indicate the boron ions. The dashed lines indicate one column of ribbons. The a coordinates of Mn1 and Mn2 within dark octahedra are the same while the clear ones differ from those by $a/2$.

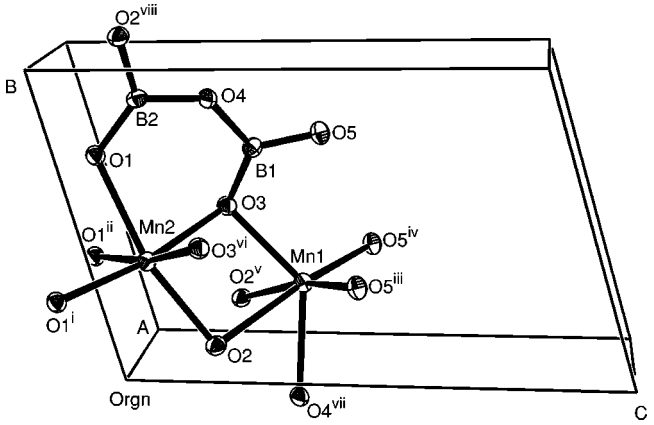

FIG. 2. ORTEP drawing of the structure fragment of pyroborate $Mn_2B_2O_5$. Ellipsoids are drawn at the 50% probability level. Symmetry codes: (i) $-x,-y+1,-z$; (ii) $-x+1,-y+1,-z$; (iii) $-x+1,-y+1,-z+1$; (iv) $-x+2,-y+1,-z+1$; (v) $x+1,y,z$; (vi) $x-1,y,z$; (vii) $x,y-1,z$; (viii) $x,y+1,z$; (ix) $-x+2,-y+1,-z$; (x) $x+2,y,z$.

random exchange Heisenberg antiferromagnetic chain (REHAC).[2] The low dimensionality in this case is clearly associated with the ribbon substructure. Disorder arises from the *random occupation of the metal sites in the ribbons* by M and M', a feature which is shared with the heterometallic pyroborates.[1] At sufficiently low temperatures, these warwickites present a crossover to 3D behavior signalled by spin-glass transitions at 2.7 K and 11 K, respectively.[3]

In this work, we show that the heterometallic pyroborate $MnMgB_2O_5$ presents a magnetic susceptibility with a power-law temperature dependence from 19 K down to the lowest temperature of our measurements (1.8 K). Its magnetization isotherm at 1.8 K also presents a power-law dependence on the applied field H, for $H>45$ kOe, as expected for a REHAC system. On the other hand, the magnetic susceptibility and electron-paramagnetic-resonance (EPR) measurements on the homometallic $Mn_2B_2O_5$, reported here, indicate that this compound is a genuine 3D antiferromagnet, i.e., its sublattice moments compensate perfectly. These results show the similarity between the magnetic behavior of pyroborates and warwickites as concerns both, heterometallic and homometallic systems. We point out, however, that no sign of weak ferromagnetism has been found in the pyroborates. We also present magnetization versus field measurements in the pyroborate $Mn_2B_2O_5$ at fixed temperatures below T_N. We have observed several inflection points in these isotherms at fields H_p, which show distinct temperature dependencies.

II. EXPERIMENT

A. The samples

$Mn_2B_2O_5$ has been synthesized from the mixture $2MnO+B_2O_3+2Na_2B_4O_7$. It was heated at 1150 °C during 24 h in Ar atmosphere and slowly cooled down to 600 °C. Below this temperature, the furnace was turned off. After the reaction product was washed in hot water, dark pink needles, circa 2 mm long, were separated individually. The material was identified through single-crystal x-ray Diffractometry.

$MnMgB_2O_5$ has been synthesized from the mixture $MgO+MnO+0.75\ K_2CO_3+0.25\ Na_2CO_3$. It has been heated at 1050 °C during 24 h in Ar flow and cooled as in the previous case. The reaction product was washed in hot water and white needles, circa 1 mm long, were separated individually. The identification of the material was done through powder x-ray diffractometry following Utzolino and Bluhm.[1] The $MnMgB_2O_5$ sample for each magnetic measurement was an ensemble of nonoriented needles weighting 50 mg. The needles of both pyroborates present equally spaced grooves in one of their faces.

B. X-ray diffractometry

A room-temperature single-crystal x-ray experiment was performed for the homometallic $Mn_2B_2O_5$ system using a crystal of dimensions $0.03\times0.05\times0.08$ mm^3. The measurements were carried out on an Enraf-Nonius Kappa charge-coupled-device diffractometer with Mo $K\alpha$ radiation. Data were collected up to 60° in 2θ, with a redundancy of 4. The structure turned out to be same as that of the heterometallic system $MnMgB_2O_5$,[1] which crystallizes in the triclinic space group $P-1$. A low-temperature experiment (100 K) was also performed in order to check for an eventual phase transition which turned out not to occur. Therefore, hereinafter all discussion is given in terms of the room-temperature structure. Crystal data, data collection procedures, structure determination methods, and refinement results are summarized in Table I.

Figure 2 shows an Oak Ridge Thermal Ellipsoid Plot Program for Crystal Structure (ORTEP) view of the asymmetric unit plus the coordination environment around Mn1 and Mn2. Some selected geometric parameters are shown in Table II. The mean B-O bond length and the mean B-O-B bond angle are in good agreement with the expected trigonal planar geometry. It is important to emphasize that the coordination around both metals is an extremely distorted octahedron, especially in the case of Mn1. The Mn-O bond lengths range from 2.068(3) to 2.413(3) Å for Mn1 and from 2.109(3) to 2.265(3) Å for Mn2. The distortions in the bond angles are much larger. The O-Mn-O angles range from 58.9(1)° to 113.5(1)° for Mn1 and from 82.4(1)° to 105.5(1)° for Mn2.

The arrangement of metals Mn1 and Mn2 gives rise to rows of Mn1 and Mn2 aligned along the a axis These rows are organized in wider ribbons rows with four metals in the order Mn1-Mn2-Mn2-Mn1 (see Fig. 1). The mean distance between the rows within the ribbons is 2.91(3) Å. The individual ribbons present an almost hexagonal network of the Mn1 and Mn2 sites with a mean separation of 3.32(5) Å (see Fig. 3 and Table II). The ribbons are also stacked along the b axis forming infinite columns (indicated in Fig. 1). The mean separation of the ribbons' planes is 4.6(1) Å while the ribbons' shift along the $(0,-1,1)$ directions is 4.300 Å. Within each column, the closest interribbons metal distances are 4.826 Å and 4.610 Å between Mn2 and Mn2 sites and 4.966 Å between Mn1 and Mn2 sites. Since Mn1 rows are at

TABLE I. Crystal data and structure refinement for $Mn_2B_2O_5$.

Temperature	297 K	100 K
System/space group	Triclinic/P-1	Triclinic/P-1
Unit-cell dimensions	$a=3.2770(1)$ Å	$a=3.26920(10)$ Å
	$b=6.2720(2)$ Å	$b=6.2717(2)$ Å
	$c=9.5880(4)$ Å	$c=9.5796(4)$ Å
	$\alpha=104.836(2)°$	$\alpha=104.840(2)°$
	$\beta=90.561(2)°$	$\beta=90.406(2)°$
	$\gamma=91.936(2)°$	$\gamma=91.949(2)°$
Z	2	2
Absorption coefficient	6.531 mm^{-1}	6.552 mm^{-1}
Reflections collected	2120	2032
Independent reflections	1118	1117
	$[R(\text{int})=0.0382]$	$[R(\text{int})=0.0418]$
Data/parameters	1118/83	1117/83
Goodness of fit on F^2	1.176	1.145
Final R indices $[I>2\sigma(I)]$	$R1=0.0345$	$R1=0.0381$
	$wR2=0.0820$	$wR2=0.0880$
R indices (all data)	$R1=0.0439$	$R1=0.0460$
	$wR2=0.1223$	$wR2=0.1118$
Extinction coefficient	0.17(2)	0.155(12)
Largest difference peak	0.977	0.925
Hole	$-0.966\,e$ Å^{-3}	$-0.925\,e$ Å^{-3}

the ribbon edges, the closest interribbons Mn1 distances take place between different columns. For coplanar ribbons, the closest distances between Mn1 sites are 4.522 Å and 4.446 Å. For ribbons in adjacent planes, the closest distances between Mn1 sites in different columns are 4.198 Å and 4.113 Å.

C. Magnetic susceptibility

Magnetization and ac susceptibility measurements were performed in a commercial magnetometer (Quantum Design PPMS). Figures 4 and 5 show the inverse of the dc magnetic susceptibility, χ_{dc}^{-1}, as a function of temperature, for powdered $Mn_2B_2O_5$ and $MnMgB_2O_5$, respectively. The Curie-Weiss law is obeyed within an extensive temperature range and the Curie-Weiss temperatures θ are negative for both systems, indicating antiferromagnetic interactions. From the Curie-Weiss law parameters, which appear in Figs. 4 and 5, the number of effective Bohr magnetons per Mn ion may be found for each compound. These are $5.84\mu_B$ and $5.38\mu_B$ for $Mn_2B_2O_5$ and $MnMgB_2O_5$, respectively, as expected.[6]

The χ_{dc}^{-1} curve for the homometallic pyroborate presents a minimum around 24 K which indicates the onset of antiferromagnetic order. This order is destroyed by a magnetic field of 50 kOe as shown in Fig. 4. Figure 6 shows the real part of the ac susceptibility, χ'_{ac}, as a function of temperature, measured with the applied field perpendicular and parallel to the axis of $Mn_2B_2O_5$ needles. This curve shows that the homometallic manganese pyroborate is a standard antiferromagnet with its easy axis perpendicular to the needle axis which coincides with the crystalline a axis. From this curve we obtain $T_N \approx 24$ K in agreement with the dc results shown in Fig. 4. The susceptibility results yield $T_N < |\theta| = 48.1$ K for $Mn_2B_2O_5$. The $|\theta|$ value is due to intraribbon superexchange interactions while the T_N value is determined by the interribbon super-superexchange, as suggested by the distances obtained from the x-ray measurements.

In the heterometallic pyroborate, χ_{dc} is proportional to $T^{-\alpha}$ below ≈ 19 K (see inset of Fig. 5). The value of this exponent obtained from the linear fitting of the $\ln \chi_{dc}$ versus $\ln T$ curve is $\alpha \approx 0.55$. This is the same as that found for the warwickite $MnScOBO_3$.[3] Notice that $MnMgB_2O_5$ is *intrinsically disordered*, as the Mg or Mn ions occupy the sites in

TABLE II. Bond lengths in Å and bond angle in degrees for ions within a ribbon in $Mn_2B_2O_5$ at room temperature (see Figs. 2 and 3).

Mn(1)-O(2)	2.413(3)	Mn(2)-O(2)	2.109(3)
Mn(1)-O(2) [a]	2.315(3)	Mn(2)-O(3) [b]	2.245(3)
Mn(1)-O(3)	2.169(3)	Mn(2) [a] -Mn(2)	3.277(3)
Mn(1)-O(4) [c]	2.260(3)	Mn(2) [a] -Mn(2) [d]	3.277(3)
Mn(1)-O(5) [e]	2.068(3)	Mn(2) [a] -Mn(2) [f]	3.371(3)
Mn(1)-O(5) [g]	2.111(3)	Mn(2) [a] -Mn(2) [h]	3.274(3)
Mn(2)-O(1)	2.265(3)	Mn(2) [a] -Mn(1) [a]	3.391(3)
Mn(2)-O(1) [i]	2.167(3)	Mn(2) [a] -Mn(1)	3.336(3)
Mn(2)-O(1) [h]	2.213(3)	B-O mean	1.37(3)
Mn(2)-O(3) [j]	2.209(3)	O-B-O mean	120(5)

[a] $x+1,y,z$.
[b] $x-1,y,z$.
[c] $x,y-1,z$.
[d] $x+2,y,z$.
[e] $-x+2,-y+1,-z+1$.
[f] $-x+2,-y+1,-z$.
[g] $-x+1,-y+1,-z+1$.
[h] $-x+1,-y+1,-z$.
[i] $-x,-y+1,-z$.
[j] $x,y+1,z$.

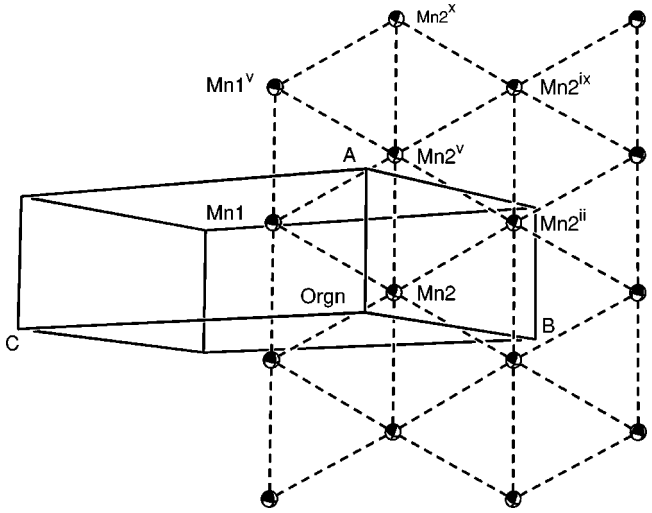

FIG. 3. Ribbon representation showing the packing of metal sites along the *a axis*. See distances in Table II.

the ribbon with equal probabilities.[1] This gives rise to the REHAC behavior, here in a system with $S=5/2$. Figure 7 shows χ'_{ac} measured on $MnMgB_2O_5$. Notice that there is no sign of magnetic phase transition in this compound down to 1.8 K.

D. Magnetization

The magnetization curve $M(H)$ for $MnMgB_2O_5$ at 1.8 K appears in Fig. 8. From the log-log plot shown in the inset we verify that $M \propto H^{\beta}$, for $H>45$ kOe, where $\beta=0.49\approx 1-\alpha$ where α is the susceptibility exponent. This result confirms the REHAC nature of this compound exhibiting a random singlet phase as discussed below.

Figure 9 shows the magnetization isotherm at 2 K measured on needles of $Mn_2B_2O_5$ with applied field perpendicular to their axis. This curve presents a slight hysteresis and some inflection points at field values H_{pn} which, although visible in the raw data, are better seen as maxima in the dM/dH versus H curve shown in Fig. 10. This figure shows

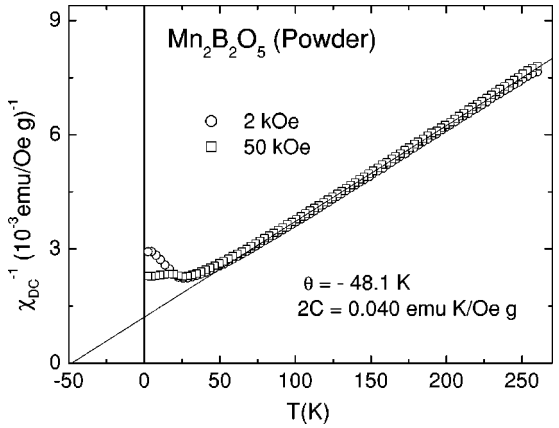

FIG. 4. Inverse of the dc susceptibility of powdered $Mn_2B_2O_5$ as a function of temperature measured under applied fields $H=2$ kOe and 50 kOe. We have taken $2C=(\chi)(T+\theta)$.

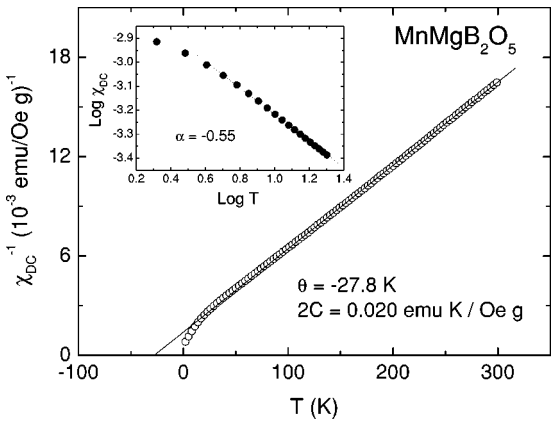

FIG. 5. Inverse of the dc susceptibility of $MnMgB_2O_5$ as a function of temperature measured under an applied field $H=10$ kOe. The inset shows the power-law behavior $\chi_{dc} \propto T^{-\alpha}$, with $\alpha \approx 0.55$. We have taken $2C=(\chi)(T+\theta)$.

the derivatives of other isotherms enabling us to observe the temperature dependence of each maximum, i.e., of $H_{pn}(T)$. The inset in Fig. 9 shows this dependence. The maximum position, at the lowest field value (H_{p1}), we identify as the critical or spin-flop field $H_c(T)$ required to destroy the 3D antiferromagnetic order. This field appears to extrapolate to zero for a temperature smaller than T_N. The other fields H_{pn} are rather temperature independent in the temperature range they can be measured. We tentatively associate these fields with those necessary to flip pairs of spins *inside* the ribbons. This is justified since there are four rows and two different crystallographic metal sites in each ribbon so that different exchange energies may exist. If the applied field is parallel to the needles' axis, these inflection points disappear. This indicates that the easy axis of magnetization is perpendicular to the needles' axis as already verified through ac susceptibility measurements. The magnetization curves for $Mn_2B_2O_5$ do not saturate for applied fields so intense as 90 kOe. Although the metal ions in the ribbons form an almost regular hexagonal lattice, see Fig. 3 and Table II, $Mn_2B_2O_5$ does not exhibit any behavior associated with frustrated systems. The reason

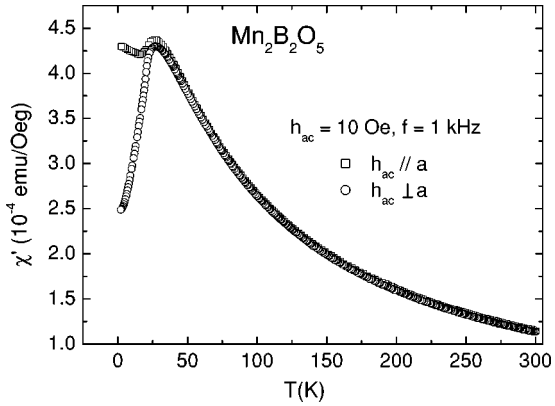

FIG. 6. Real part of the ac susceptibility, χ'_{ac}, of $Mn_2B_2O_5$, as a function of temperature measured under an alternating field h_{ac} with amplitude of 10 Oe and frequency of 1 kHz. Squares (circles) indicate h_{ac} parallel (perpendicular) to the crystallographic *a* axis.

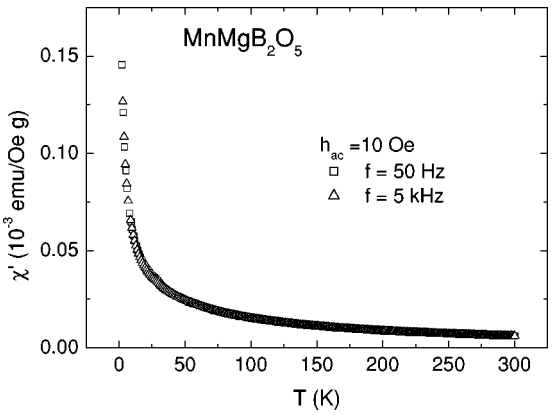

FIG. 7. Real part of the ac susceptibility, χ'_{ac}, of $MnMgB_2O_5$, as a function of temperature measured under alternating fields h_{ac} with amplitude of 10 Oe and frequencies of 50 Hz (squares) and 5 kHz (triangles).

is that there is always an antiferromagnetic interaction that dominates the others. Different intensities arise, since the oxygens which mediate such interactions form octahedra with different degrees of distortion around the Mn sites (see Fig. 2). Notice also that $T_N < |\theta|/2$ for $Mn_2B_2O_5$, a feature usually attributed to geometrical frustration but that in this system is due to the low dimensionality of the subunits in the crystal structure.[8]

E. EPR

EPR measurements were performed on a single needle of $Mn_2B_2O_5$ employing a 9.5 GHz Brucker spectrometer. The lowest temperature for which it was possible to observe a spectrum was $T=24.4$ K$\approx T_N$ which led us to conclude that this material is a genuine antiferromagnet for low temperatures. Above 24.4 K, the observed spectrum consists of a single intense, broad, and symmetric line. If the applied field is perpendicular to the needle axis, the center of the spectrum is at $g=1.992$. For the parallel configuration its center is at $g=2.045$. Figure 11 shows the observed linewidth ΔH as a function of temperature. In the inset we plot $\ln(\Delta H)$ versus $\ln(T-T_N)$. A linear fitting has been done for different T_N values. The smallest square deviation was obtained for $T_N=23.3$ K. For this value of T_N, the slope γ of the straight line is -0.42 so that the linewidth diverges as $\Delta H \propto |T-T_N|^{-0.42}$ as the temperature approaches T_N. The rapid increase in ΔH as T decreases from about $2T_N$ indicates the development of long-range antiferromagnetic spin ordering. We point out for comparison that the value of the linewidth exponent for MnF_2 is -0.38.[9] Theoretically, in the case anisotropy can be treated as a small perturbation as for the present system, this exponent is given by $-(1/2)(7+\eta)\nu - 2(1-\alpha)$ where we use the conventional notation for the critical exponents.[10] Using $\eta=\alpha=0$ and $\nu=2/3$, appropriate for a $3d$-Heisenberg system, we find the value $-1/3$ for the linewidth exponent. This gives a rather weaker divergence than that measured here.

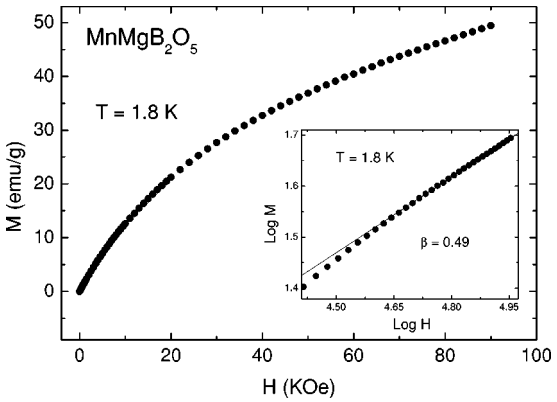

FIG. 8. Magnetization isotherm for $MnMgB_2O_5$ at 1.8 K. The inset shows the power-law behavior $M \propto H^{\beta}$, for $H>45$ kOe where $\beta \approx 0.49$.

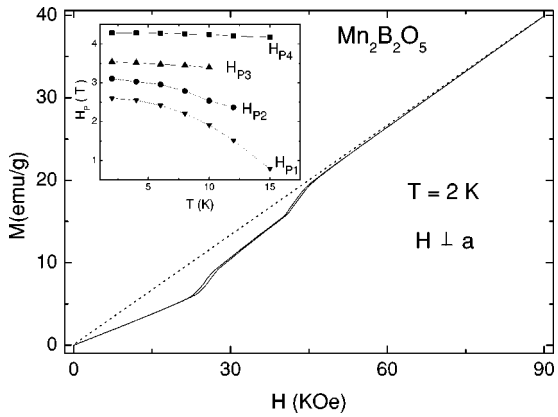

FIG. 9. Magnetization isotherm for $Mn_2B_2O_5$ at 2 K measured with applied field perpendicular to the *a axis*. Notice the slight hysteresis. The dashed line is a guide for the eyes. The inset shows the temperature dependence of the inflection points H_{pn} (see Fig. 10).

III. DISCUSSION

A. Magnetic dimensionality

The crystalline structure of the pyroborates may be considered as a bundle of ribbons formed by oxygen octahedra

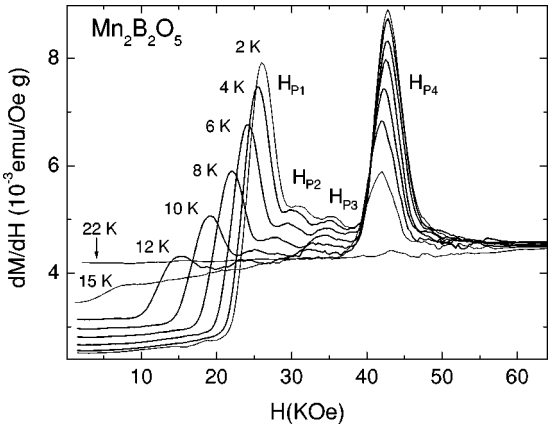

FIG. 10. Derivatives of several magnetization isotherms for $Mn_2B_2O_5$ measured with increasing field. The maxima define the H_{pn} values.

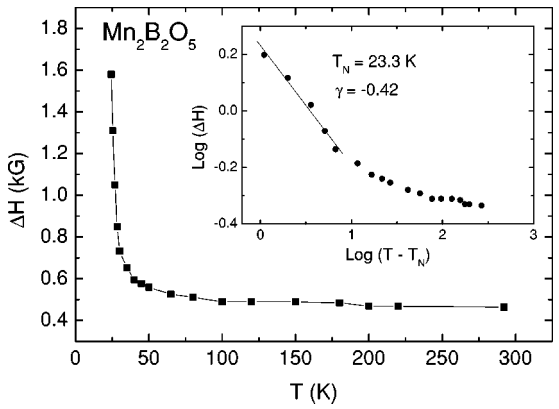

FIG. 11. Temperature dependence of the EPR linewidth for the applied field parallel to the needle axis, i.e., perpendicular to the easy axis of magnetization. The inset shows a fitting of the function $\ln(\Delta H)=\gamma\ln(T-T_N)$ to the experimental data.

held together by the borate groups. In this structure, the ribbons do not *touch* so that the interribbon magnetic interactions may exist only through the super-superexchange mechanism. This is different from the warwickites where the ribbons are closer together and explains why the Neel temperature of the homometallic pyroborate $Mn_2B_2O_5$ is smaller than that of the homometallic warwickite Mn_2OBO_3 even if the Curie-Weiss temperatures in both systems are comparable. In fact the 3D ordering is due to the interribbon interactions, which is weaker in the former system. Table III compares T_N of the Mn pyroborate with those of other 3D manganese compounds such as MnF_2 and $MnRbF_3$.

On the other hand, the heterometallic pyroborate $MnMgB_2O_5$ is clearly a one-dimensional system dominated by the intrinsic disorder due to the random occupation of the two sites of the ribbon by different metals in the same proportions.[1] This severely weakens the interribbon interactions so that $MnMgB_2O_5$ behaves as a REHAC system with a random singlet phase and no order down to the lowest temperature of our measurements ($T=1.8$ K). The random singlet phase is made evident from the temperature dependence of the susceptibility, $\chi(T)\propto T^{-\alpha}$ for T below 19 K. Furthermore, the M versus H measurements at fixed $T=2$ K show that $M\propto H^{\beta}$, for $k_BT<g\mu_BSH<g\mu_BSH_E$, where H_E is the maximum exchange field defined in Eq. (3) below and $\beta\approx 1-\alpha$. In order to understand the REHAC behavior in $MnMgB_2O_5$, in spite that we have site disorder in this material, it is essential to consider that the superexchange interactions extend beyond nearest-neighbor metal ions through several different oxygen octahedra belonging to the same and to adjacent columns. As these octahedra have different distortions, depending on the metal ion inside them, the superexchange interactions are in fact random. The magnetization and susceptibility of $MnMgB_2O_5$ have the same behavior as those of the heterometallic warwickite[2] $MgTiOBO_3$, which is the paradigm of the inorganic REHAC compounds with a random singlet phase. However, in the latter material, Ti^{3+} has $S=1/2$ while in the present system the magnetic ion is Mn^{2+} whose electronic configuration is $(3d^5)$ with $S=5/2$. There is an intense discussion nowadays on the existence and the nature of random singlet phase in REHAC systems with S larger than 1/2.[11,12] Our experiments make evident conventional random singlet-phase behavior in a REHAC system with $S=5/2$.

TABLE III. Magnetic parameters for some manganese compounds (Ref. 7). The meaning of the symbols are in the text.

Compound	T_N (K)	H_c (kOe)	H_A (kOe)	H_E (kOe)
$Mn_2B_2O_5$	23.3	26	0.4	358
MnF_2	74	93	8.4	515
$RbMnF_3$	82	2.7	0.0045	830

B. Anisotropy and exchange

We assume that, in $Mn_2B_2O_5$, the critical field for the spin-axis flopping, H_c, is given by that yielding the first maximum (H_{p1}) in Fig. 10, i.e., that which is found at the lowest field value and shows the strongest temperature dependence. The anisotropy energy K is given by

$$K(T)=\frac{1}{2}H_c^2[\chi_\perp-\chi_\parallel]. \tag{1}$$

Substituting the experimental values in this expression yields $K(2K)=61.3$ kergs/g. The anisotropy field H_A can be obtained from the equation.[13]

$$H_A=\frac{K}{M_s} \tag{2}$$

and the value of the sublattice magnetization, $M_s=154.1$ ergs/Oe g. We get $H_A=0.4$ kOe. The exchange field H_E is given by

$$H_E=\frac{M_s}{\chi_\perp}. \tag{3}$$

From this equation and the experimental value of $\chi_\perp$, we obtain $H_E=358$ kOe. The above results show that $Mn_2B_2O_5$ is an antiferromagnetic material with moderate exchange interaction and low anisotropy in agreement with the S character of the Mn^{2+} ion. Table III gives T_N, H_c, H_A, and H_E for this and other 3D manganese compounds. The low dimensionality of the ribbons joining to form the 3D structure is manifested in a T_N, due to interribbon interactions, which is nearly half the Curie-Weiss temperature which in turn is associated with intraribbon interactions. Also, the other maxima in Fig. 10 indicate stronger exchange interactions, probably originated from intraribbon pairs for which the intermetallic distances are smaller. We remark that low dimensionality is a general requirement for a system to exhibit steps in the magnetization isotherms.[14]

In conclusion, we have shown that the low-dimensional ribbon substructures, which join to form the 3D pyroborates, strongly influence and even determine the magnetic properties of these systems. The homometallic $Mn_2B_2O_5$ presents a low Neel temperature and magnetization steps as conse-

quences of such substructures. The heterometallic compound presents a REHAC behavior due to the random occupation of the sites by the magnetic ions in the disconnected ribbons. Our results in $MnMgB_2O_5$ provide strong evidence for a random singlet phase in $S=5/2$ REHAC systems.

ACKNOWLEDGMENTS

This work has been supported by the Brazilian agencies FAPERJ, CNPq, FAPESP, and CNRS (France). Dr. C.O. Paiva-Santos has taken the x-ray diffractogram from $MnMgB_2O_5$ at the LIEC-UNESP.

*Electronic address: mucio@if.uff.br

[1] A. Utzolino and K. Bluhm, Z. Naturforsch., B: Chem. Sci. **51**, 912 (1996), and references therein.

[2] J.C. Fernandes, R.B. Guimarães, M.A. Continentino, H.A. Borges, J.V. Valarelli, and Alex Lacerda, Phys. Rev. B **50**, 16 754 (1994).

[3] R.B. Guimarães, J.C. Fernandes, M.A. Continentino, H.A. Borges, C.S. Moura, J.B.M. da Cunha, and C.A. dos Santos, Phys. Rev. B **56**, 292 (1997).

[4] See R. Norrestam, M. Kritikos, and A. Södin, J. Solid State Chem. **114**, 311 (1995).

[5] M.A. Continentino, A.M. Pedreira, R.B. Guimarães, M. Mir, J.C. Fernandes, R.S. Freitas, and L. Ghivelder, Phys. Rev. B **64**, 014406 (2001).

[6] See George Pake, *Paramagnetic Resonance* (Benjamin, New York, 1962), p. 9.

[7] F. Keffer, *Spin Waves*, edited by S. Fluge, Handbuch der Physik Vol. XVIII/B, (Springer-Verlag, Berlin, 1966).

[8] S.T. Bramwell and M.J.P. Gingras, Science **294**, 1495 (2001); P. Schiffer and A.P. Ramirez, Comments Condens. Matter Phys. **18**, 21 (1996).

[9] J.C. Burgiel and M.W.P. Strandberg, J. Phys. Chem. Solids **26**, 865 (1965).

[10] K. Kawasaki, Phys. Lett. **26A**, 543 (1968).

[11] G. Refael, S. Kehrein, and D.S. Fisher, Phys. Rev. B **66**, 060402 (2002).

[12] A. Saguia, B. Boechat, and M.A. Continentino, Phys. Rev. Lett. **89**, 117202 (2002).

[13] See S. V. Vonsovskii, *Magnetism* (Wiley, New York, 1974), p. 864.

[14] H. Kobayashi and T. Haseda, J. Phys. Soc. Jpn. **19**, 765 (1964).